HEAT, AIR, AND MOISTURE TRANSFER IN ENVELOPE PARTS: THE INTERNATIONAL ENERGY AGENCIES ANNEX 24 COMMON EXERCISES

Hugo Hens, S.L.C.

ABSTRACT

Annex 24 of the International Energy Agency, Executive Committee on Energy Conservation in Buildings and Community Systems—Heat, Air and Moisture Transfer in Highly Insulated New and Retrofitted Envelopes—was initiated in 1991. Fourteen countries joined together to study the physics of heat, air, and moisture transfer and to analyze the consequences for energy use, hygric response, and durability. The annex contained five subtasks, one of them being modeling. This subtask not only included a state-of-the-art review and model development but also model verification through the solution and discussion of six common exercises: a concrete flat roof, a timber-framed wall, a cavity wall, an industrial metallic roof, a timber flat roof cassette, and a crawl space.

The exercise results taught that, in general, models of the same level of comprehensiveness give comparable qualitative predictions. Nearly full models also produce much richer and better information than simple tools do. Numerical differences between model predictions, however, remain important. In many cases, scatter starts with the interpretation of boundary conditions. Further differences are attributed to the use of different functional forms for the same material property, different simplifications in geometry, and the intrinsic incompleteness of each particular model.

The conclusion of the verification exercise is that, today, it is possible to calculate the hygrothermal behavior of envelope parts in a qualitatively correct way, at least if models are applied that consider all aspects of combined heat, air, and moisture transfer. This supports model use for performance control.

INTRODUCTION

The motivation of the International Energy Agency Executive Committee on Energy Conservation in Buildings and Community Systems to start an annex on heat, air, and moisture transfer in highly insulated new and retrofitted envelopes was twofold. First, as insulation requirements become more strict, the impact on thermal quality of secondary effects such as enthalpy flow, latent heat, and moisture-affected thermal conductivity increases. Second, an enquiry underlined that codes of practice in many member states of the International Energy Agency treat heat, air, and moisture design in an unsatisfactory way compared to the level of scientific knowledge available. The annex was initiated in 1991. Fourteen countries joined the common research: Belgium (operating agent), Canada, Denmark, Finland, France, Germany, the Netherlands, Norway, Italy, Slovakia, Sweden, Switzerland, the United Kingdom, and the United States. Five subtasks were defined: (1) modeling, (2) environmental conditions, (3) material properties, (4) experimental verification, and (5) practice (Anon. 1991). Subtask 1, modeling, started with an enquiry on existing heat, air, moisture, and computer-aided tool codes (HAMCaT), (Hens and Janssens 1992). Then, it focused on specific topics such as transfer potentials, contact conditions, and airflow modeling. Simple engineering methods were analyzed and the concept of simplified modeling was developed: equations close to the full physical model and material properties gained from simple, standardized measurements. Last but not least, the subtask organized a model verification project through the formulation and solution of six common exercises.

HEAT, AIR, AND MOISTURE TRANSFER MODELS

Short Recapitulation

Heat, air, and moisture transfer models are based on the conservation of energy, mass, and momentum axioms, which state that the resulting inflow or outflow of heat, mass, and momentum in an elementary volume,

Hugo Hens is a professor of building physics in the Department of Civil Engineering at the Catholic University of Leuven, Belgium.

together with the local rate of generation or absorption, equals the change rate in amount of energy, mass, and momentum in the volume. In vector analysis, inflow or outflow per unit volume is called a *divergence* (div). Consequently, the three conservation laws state:

$$\text{div (Flux)} \pm S = -\frac{\partial (\text{content})}{\partial t}. \quad (1)$$

Heat, water vapor, and water fluxes concern two separate categories: diffusive and convective. Diffusive fluxes, such as heat conduction, water vapor diffusion, and unsaturated water flow, are defined by the product of a transport property and the gradient of a driving force (in vector notation: grad). The driving force for heat flow is temperature, for water vapor flow it is partial vapor pressure, and for water flow it is total suction:

$$\begin{aligned} &\text{heat} \quad \dot{q} = -\lambda \, \text{grad} T \\ &\text{vapor} \quad \dot{m}_v = -\delta \, \text{grad} p \\ &\text{water} \quad \dot{m}_m = -k_w \, \text{grad} s. \end{aligned} \quad (2)$$

Thermal conductivity (g), vapor permeability (δ), and water permeability (k_w) introduce the medium wherein transport takes place. The difficulty is that these properties are not constants, but functions of the driving forces and stored quantities such as moisture content.

Convective fluxes relate to the energy, called enthalpy, embodied in each mass component and displaced with it, and the water vapor movement caused by airflow:

$$\begin{aligned} &\text{Enthalpy} \quad \dot{q} = \dot{m} h \\ &\text{Vapor} \quad \dot{m}_v = \dot{m}_a X. \end{aligned} \quad (3)$$

Vapor and moisture fluxes in envelope assemblies are so small that the momentum displacement they cause can be disregarded. This also holds for air transport in porous materials:

$$\dot{m}_a = -k_a \, \text{grad} \, (p_a - \rho g z). \quad (4)$$

The driving force ($p_a - \rho g z$) in diffusive equation 4 is total air pressure, corrected on stack effect. k_a represents the air permeability of the material. In leaks, cracks, overlays, and air spaces, however, air velocity may be such that momentum cannot be neglected anymore. This complicates the description of air transport considerably.

A last set of relations used in heat, air, and moisture models are the equations of state: saturation pressure as a function of temperature and capillary radius, enthalpy as a function of temperature and phase change, the sorption isotherms, and the suction characteristics of the materials used. These relations couple stored mass and stored energy to driving forces. In doing that, a second set of material properties emerges: the volumic-specific capacities for heat, water vapor, water, and air. At the same time, the relations interlink driving forces, with the consequence that each set of potentials can be transformed into another set, provided that the transport properties and volumic-specific capacities are also transformed. A driving force can even be split into two forces. An example is vapor pressure (p), which is presented by the product of relative humidity and vapor saturation pressure. Saturation pressure, in turn, depends on temperature.

Combining the conservation laws with the preceding flux expressions and equations of state results in a set of at least three scalar partial differential equations (PDEs), called the model equations. An example is

$$\begin{aligned} &\text{div} \, \dot{m}_a = 0 \\ &\text{div} \, (\delta \, \text{grad} p - \dot{m}_a X + k_w \, \text{grad} s) \pm S_M = \frac{\partial w}{\partial t} \\ &\text{div} \, (\lambda \, \text{grad} T - \dot{m}_a c_a T - \dot{m}_v l_b) \pm S_Q = \frac{\partial h_T}{\partial t}. \end{aligned} \quad (5)$$

(1) (2) (3)

where w is the moisture content and h_T is the specific enthalpy of the porous skeleton, including the mass content of the pores. The first equation states that the air response is instantaneous under transient conditions. The second equation expresses conservation of moisture, i.e., the sum of water vapor and water, for temperatures above 0°C. The third equation explains that not only conduction (1) but also air-induced enthalpy flow (2) and latent heat (3) play a role in heat transport and storage. The free choice of driving forces explains why various authors propose apparently different models that give comparable answers when applied in practice.

Solving the system of PDEs demands numerical techniques. Popular are finite-element and control volume methods. Geometry, initial conditions, boundary conditions, and contact conditions between materials also should be known.

Simple calculation tools dismantle system 5 in a straightforward way. Time as an independent variable is eliminated. Heat transfer concerns conduction only. Mass transfer is restricted to vapor flow by diffusion. Thermal conductivity and vapor permeability are taken as constants. Multilayered elements act as ideal flat systems. On the other hand, simplified models, as defined within the context of the annex, use the basic equations but replace the complex property functions with uniform relations deduced from simple standardized measurements.

Models offer many advantages. One of the important virtues is their potential to short-circuit time-consuming hygrothermal tests on components. In a fraction of time, a picture of what could be expected is generated and a parameter analysis is done. Models also help in a

correct interpretation of measured data. In manufacturing of components, models guide the performance controls. They help in formulating performance criteria and design rules for building practitioners. New designs can be checked. Damage cases also are better understood.

The Need for Validation

While conservation of energy, mass, and momentum belongs to the axioms of classic physics, the flow equations remain empirical statements. Both introduce material properties. Of these, thermal conductivity and specific heat capacity are measured within narrow margins. Deviations between samples of the same material stay within percentages, and dependence of governing driving forces is smooth. Hence, this is not true for hygric and air-related properties. Round-robin tests on samples of the same material give a large scatter in permeabilities, diffusivities (diffusivity being the ratio between permeability and volumic-specific capacity), and "permeability vs. driving force" relations (Galbraith et al. 1991; Kumaran 1992a). In addition, even when measured transient moisture profiles are distributed among laboratories, derived diffusivities may differ substantially (Kumaran 1992b).

Geometry of an envelope part is a complex reality. In any case, each part is three dimensional. Cracks in a material layer, overlays between built-in foils, thin air voids between layers, and joints between stiff insulation boards may all have large influences on heat, air, and moisture response. Overlooking their presence inevitably leads to simplifications, the ultimate one being the reduction of the real system to an ideal one-dimensional multilayered wall.

Even measured environmental conditions induce uncertainties: air temperature and relative humidity, measured in one point, are extrapolated over a whole surface. Local air pressures are calculated from some scarce measurements or general data from the literature. Precipitation is only known on a daily basis. Measuring devices demonstrate limited accuracy. Also, starting conditions may be quite diffuse. Surface coefficients are simplified to constants, etc.

The first aim of any partial verification, therefore, is to prove that these simplifications and uncertainties do not falsify predictions to such an extent that the results become wrong. Detailed verification, of course, also has a quantitative objective: showing that numerical values for flows, driving force fields, and stored quantities are within acceptable margins, compared to the reference.

Methodology

Verification is based on a combination of three partial techniques: analytical verification, intermodel comparison, and empirical verification (Lomas 1994). Analytical verification is a good choice for testing algorithms. However, analytical solutions for heat and mass transfer only exist for simple cases, where material properties are constants. The fact that a model produces correct answers for constant properties is no guarantee that it does so for cases with variable properties. Intermodel comparison delivers a relative verification against an average. The temptation exists to quote a model positively when its numerical results are close to that average. However, if by accident the majority of models in the test perform poorly, the procedure is of no value. Empirical verification seems the most convenient one. However, errors in measured data or a lack of data may confuse the procedure.

Verification techniques include a visual comparison of graphs, a detailed analysis of average differences and standard deviations, and a statistical evaluation of differences between reference and calculated data on the basis of the following relation:

$$\text{Data}_{\text{calculated}} = a \cdot \text{Data}_{\text{reference}} + b. \qquad (6)$$

If both data sets are identical, then $a = 1$, $b = 0$, $\sigma_a = 0$, and $\sigma_b = 0$. The annex concentrated on the second partial verification technique (intermodel comparison) and, to some extent, on empirical verification. The vehicles used to perform the activity were the six common exercises.

THE SIX EXERCISES

With the exercises, responses were sought on five questions: (1) how good are simple engineering tools? (2) how important is the influence of air transport? (3) what are the consequences of initial moisture? (4) does driving rain have an influence on hygrothermal behavior? and (5) what about latent heat exchanges? Solutions, obtained by the participating countries, were mailed to the organizing country, which produced an intermodel comparison and did, if included in the exercise, the experimental verification.

Exercise 1: Concrete Flat Roof

Data Common exercise 1, proposed by Belgium, was of the intermodel comparison type (Hens 1991, 1992). The objective of the exercise was to evaluate the consequences of a high initial moisture content and subsequent latent heat exchanges. The roof consisted of (from inside to outside): an acoustic ceiling of aluminum laths, measuring 9 cm (3.54 in.) wide, mounted with open joints of 1 cm (0.394 in.) and covered on top with a mineral fiberboard, $d = 3$ cm (1.18 in.); air space measuring 60 cm (23.6 in.) high; post-stressed concrete slab measuring 25 cm (9.84 in.) thick; expanded clay concrete screed having a mean thickness of 15 cm (5.9 in.), with a cement finish of 2 cm (0.787 in.) (the screed is a concrete layer poured on top of the load-bearing floor, with a small slope to drain the roof); x cm (in.) of dense mineral fiber insulation, x to be calculated from $U \leq 0.25$ W/(m^2·K);

and two layers of styrene-butadiene-styrene (SBS)-polymer bitumen ply (see Figure 1a). Material properties are given in Table 1. The table gives an impression of the amount and quality of data needed to perform a simulation. Initial conditions included precipitation data during the month before and the moisture content in the screed and mortar finish the day the membrane was applied. Climates imposed were 21°C, 60% RH indoors and either the Belgian monthly average reference year for condensation or the local thermal reference year (TRY) outdoors.

Expected Response Excess water and precipitation the month before built up a high moisture content in the prestressed concrete and the lightweight aggregate screed. As observed during field investigations, this induces a redistribution of moisture in the roof structure after the membrane is applied, with the mineral fiber getting wet and staying wet for a long time (many years). One of the consequences could be an important increase in the U-factor caused by latent heat exchange the first year, followed by a decrease in the following years to an equilibrium value slightly higher than the standard U. Another consequence may be degradation of the mineral fiber.

Qualitative Verification of Simulation Results Ten reports with solutions were received. Two solutions used the Glaser method (Glaser 1958). This simple engineering tool answered with "no problem" when the

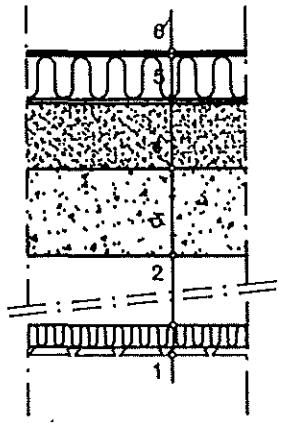

Exercise 1: concrete flat roof

1. acoustical ceiling
2. air space
3. post-stressed concrete slab, d=20 cm
4. lightweight concrete screed, d=15 cm
5. mineral fibre boards, d= x cm
6. membrane

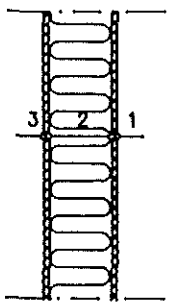

Exercise 2: timber framed wall

1. chip-board, d=12 mm
2. mineral fibre insulation, d=15 cm
3. wood fibre board, d=12 mm

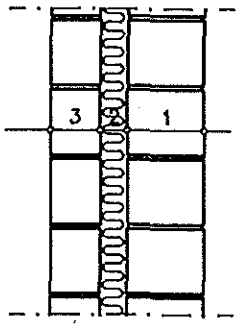

Exercise 3: cavity wall

1. lime-silicate inner leaf, d=17.5 cm
2. mineral fibre insulation, d=6 cm
3. lime-silicate outer leaf, d=11.5 cm

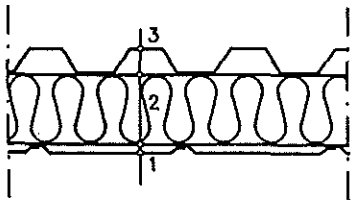

Exercise 4: metallic roof

1. interior steel liner tray
2. fibreglass-quilt, d=8 cm
3. steel profiled cladding

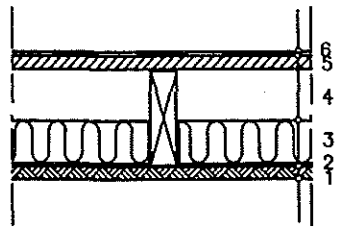

Exercise 5: timber flat roof

1. wood wool cement board, d=25 mm
2. vapour retarder (PE or a water permeable type)
3. mineral fibre, d=10 cm
4. cavity
5. plywood deck, d=12.5 mm
6. membrane

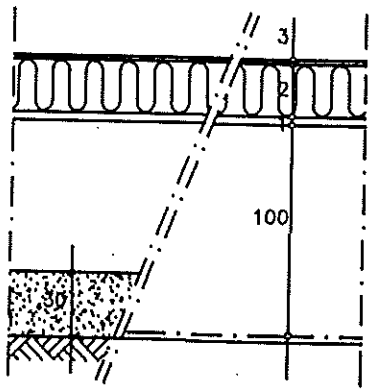

Exercise 6: crawl space

1. hardboard, d=6 mm
2. fibreglass-quilt, d=22 cm
3. timber flooring, d=22 mm
4. PE-ground-cover or lightweight aggregate loose fill

Figure 1 *The six envelope parts, analyzed in the common exercises.*

TABLE 1 Exercise 1: Material Properties

w in kg/m³; u in %kg/kg; ϕ in %

Material	Property	Value Function	Units
aluminum	density	2700	kg/m³
	dry specific heat capacity	880	J/(kg·K)
	thermal conductivity	230	W/(m·K)
mineral fiber	density	70	kg/m³
	dry specific heat capacity	840	J/(kg·K)
	thermal conductivity	0.037	W/(m·K)
	vapor permeability	$1.5\ 10^{-10}$	s
prestressed concrete	density	2200	kg/m³
	dry specific heat capacity	840	J/(kg·K)
	thermal conductivity	$2.7+0.0032w$	W/(m·K)
	sorption isotherm	$\phi/(-0.0007\phi^2+0.081\phi+0.4)$	kg/m³
	critical moisture content	100	kg/m³
	capillary moisture content	110	kg/m³
	saturation	160	kg/m³
	vapor permeability	$1.55\ 10^{-12}+2.8\ 10^{-21}\exp(0.25\phi)$	s
	water sorption coefficient	0.018	kg/(m²·s)
no-fines concrete	density	1000	kg/m³
	dry specific heat capacity	840	J/(kg·K)
	thermal conductivity	$0.37+0.001w$	W/(m·K)
	sorption isotherm	$\phi/(0.00047\phi^2+0.055\phi+0.63)$	kg/m³
	critical moisture content	140	kg/m³
	capillary moisture content	190	kg/m³
	saturation	584	kg/m³
	vapor permeability	$1.27\ 10^{-11}+1.9\ 10^{-16}\exp(0.14\phi)$	s
	water sorption coefficient	0.08	kg/(m²s½)
mortar	density	1800	kg/m³
	specific heat capacity	840	J/(kg·K)
	thermal conductivity	$0.85+0.0045w$	W/(m·K)
	sorption isotherm	$\phi/(-0.00056\phi^2+0.059\phi+0.34)$	kg/m³
	capillary moisture content	280	kg/m³
	saturation	315	kg/m³
	vapor permeability	$1.46\ 10^{-11}+2.34\ 10^{-13}\exp(0.045\phi)$	s
	water sorption coefficient	0.12	kg/(m²s½)
mineral fiber	density	175	kg/m³
	specific heat capacity	840	J/(kg·K)
	thermal conductivity	$0.038+3.2\ 10^{-5}w+5.9\ 10^{-7}w^2$	W/(m·K)
	vapor permeability	$1.5\ 10^{-10}$	s
membrane	density	1150	kg/m³
	specific heat capacity	1700	J/(kg·K)
	thermal conductivity	0.2	W/(m·K)
	vapor permeance	$1.85\ 10^{-12}$	s/m

exterior environmental conditions included solar radiation, except for some little condensation between insulation and membrane each winter, followed by complete drying in summer. Without solar radiation, some accumulation of condensate in the mineral fiber occurred. Quantities, however, are extremely low.

All other solutions using simplified or near-full models predict the response as expected: important accumulation of initial moisture in the mineral fiber and a large increase in U-factor the first year by latent heat release in the insulation. One solution, however, used an erroneous physical modeling of the mineral fiber and another applied erroneous material properties, resulting in fast drying of the concrete slab and screed. Both were eliminated for further analysis.

Numerical Verification of Simulation Results A few comparisons are summarized in Table 2. Variations on the thickness of the mineral fiberboard are mainly caused by the different standard λ-values in use in the participating countries. Standard deviations on the increase ΔU, on moisture accumulation in the mineral fiber, and on its yearly amplitude are caused by differences in exterior climatic data, differences in initial moisture content, and differences in the way noncapillary materials were modeled. Figure 2 gives an example of moisture buildup in the mineral fiber as predicted by three models.

TABLE 2 Common Exercise 1: Insulation Thickness, Increase in U-Factor During the First Year, Moisture Accumulation in the Mineral Fiber After 10 Years (Ukkel Climate, Belgium)

	Average (10 Reports)	Standard Deviation %
Insulation thickness	138.5 mm	7
Increase in U-factor the first year (U_o = 0.214 W/(m²·K))	0.126 W/(m²·K)	43
Moisture accumulation in the mineral fibre after 10 years	16.0 kg/m²	26
Amplitude of the yearly oscillation in moisture accumulation in the mineral fibre	3.1 kg/m²	47

Exercise 2: Timber-Framed Wall

Data Common exercise 2, proposed by Finland, was of the intermodel comparison type (Ojanen and Salonvaara 1992a, 1992b). The objective of the exercise was to quantify the effects of air exfiltration. The timber-framed wall consisted of an interior 12 mm (0.47 in.) thick chip-board, 150 mm (5.9 in.) of mineral fiber insulation, and an exterior 12 mm (0.47 in.) thick woodfiber-

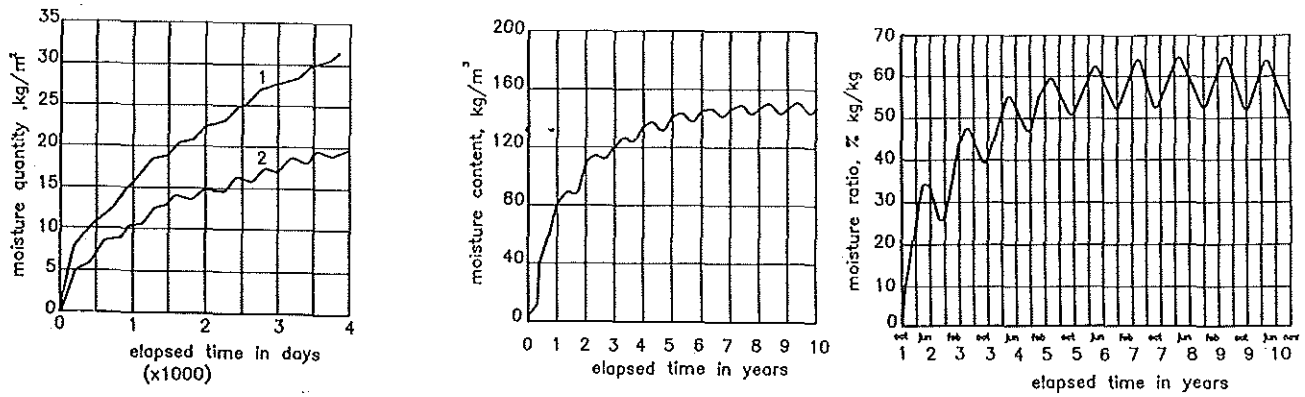

Example 1 total moisture in kg/m², (multiply with 6.67 for moisture content in kg/m³) curve 1: without solar gains curve 2: with solar gains

Example 2 moisture content in kg/m³

Example 3 moisture ratio in %kg/kg (multiply with 1.8 for moisture content in kg/m³)

Figure 2 Exercise 1, moisture accumulation in the mineral fibre under Belgian reference outdoor climate, three examples of calculated results.

TABLE 3 **Exercise 2: Material Properties**

	w in kg/m³; u in %kg/kg; ϕ in -		
Material	**Property**	**Value Function**	**Units**
wood chip-board	density	700	kg/m³
	specific heat capacity	2100	J/(kg·K)
	thermal conductivity	0.14	W/(m·K)
	sorption isotherm	$0.27+202.6\phi-486\phi^2+441\phi^3$	kg/m³
	capillary moisture content	400	kg/m³
	saturation	700	kg/m³
	vapour permeability	$\phi<0.4$ $4.6\ 10^{-12}$	s
		$\phi\geq0.4$ $(8.4-30.6\phi+6.3\ 10^{-3}(100\phi)^2 -2.5\ 10^{-5}(100\phi)^3)\cdot10^{-12}$	s
mineral fibre	density	20	kg/m³
	dry specific heat capacity	840	J/(kg·K)
	thermal conductivity	$0.0345+3.2\ 10^{-5}w+5.9\ 10^{-7}w^2$	W/(m·K)
	vapour permeability	$1.4\ 10^{-10}$	s
wood fibre board	density	280	kg/m³
	dry specific heat capacity	2100	J/(kg·K)
	thermal conductivity	0.05	W/(m·K)
	sorption isotherm	$\phi<0.68$ 32ϕ	
		$\phi\geq0.68$ $30-59\phi+69.2\phi^2$	kg/m³
	capillary moisture content	400	kg/m³
	saturation	750	kg/m³
	vapour permeability	$\phi<0.25$ $7.6\ 10^{-12}$	s
		$\phi\geq0.25$ $(51.5\phi-5.27)\cdot10^{-12}$	s

board. No further exterior cladding was applied (Figure 1b). Material properties are given in Table 3. A weather data file for Ottawa was used, with the indoor climate being 20°C and 40% RH. Four cases were considered: wall airtight, separate constant ventilation flow of 1 L/(m²·s); wall airtight, separate wind-induced ventilation flow; wall air permeable, constant exfiltration rate of 1 L/(m²·s); and wall permeable, variable ex- or infiltration rate induced by wind. All four were simulated with and without solar gains.

Expected Response As experienced in hot-box measurements, air exfiltration should have two important consequences: a large part of the heat loss through the wall caused by enthalpy flow and moisture accumulation by interstitial condensation reaching much higher values than in the diffusion mode. The second consequence, of course, depends largely on the specific climatic conditions.

Qualitative Verification of Simulation Results Seven reports with solutions were received. The simple Glaser method, with its inability to handle air exfiltration, quoted the construction as well insulated and completely condensation free, even for the severe Ottawa outdoor climate.

Solutions, using simplified or near-full models with an air transfer module, were in good agreement with the expectations. Enthalpy flow overrules conduction as a heat loss mechanism. Moisture accumulation in the wall during winter remains low in the diffusion mode but increases to high values when exfiltration is active.

Numerical Verification of the Simulation Results Table 4 and Figure 3 compare the results for the heat losses on a yearly basis and for total moisture accumulation for the case with a constant exfiltration rate. Losses by enthalpy flow are identical between reports. Conductive flow, however, shows large discrepancies. One report even predicts heat gains, while all others give losses. Moisture accumulation is excessively high in one report: 51.1 kg/m², all in the insulation. The four other reports scatter between 10.6 and 26 kg/m², with the

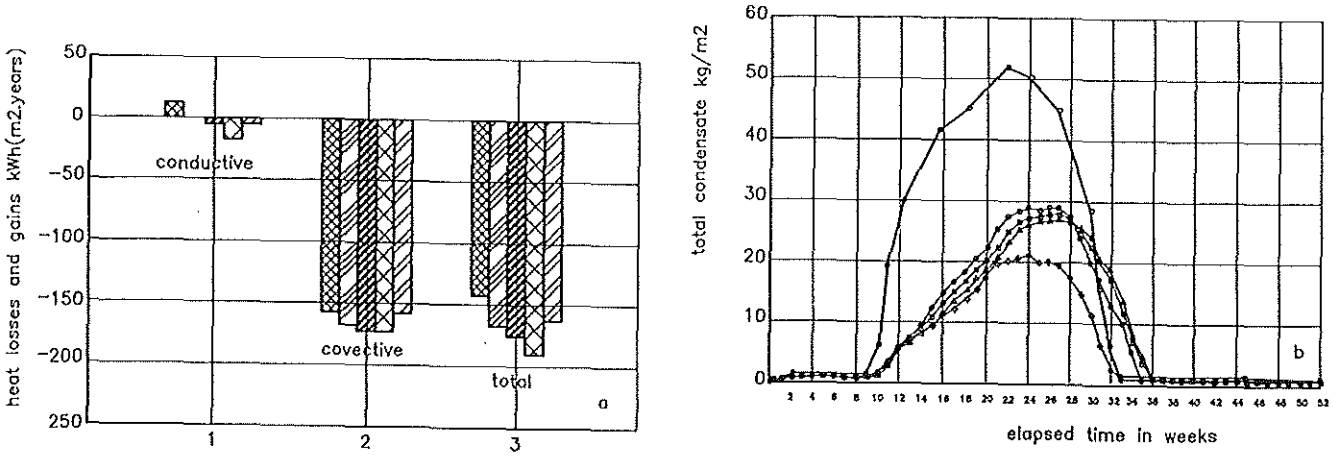

(a) Each bar represents a different simulation result

(b) Each line represents a different simulation result

Figure 3 *Exercise 2, air exfiltration: (a) heat losses in kWh/(m²·year) and (b) total condensate in the timber framed wall under Ottawa climate conditions*

TABLE 4 **Common Exercise 2: Heat Losses on Yearly Basis, Moisture Accumulation in Winter, Case with Constant Exfiltration Rate (Ottawa Climate, Canada)**

	Average (6 Reports)	Standard Deviation %
Heat loss by convection	163.5 kWh/m²	5
Heat loss by conduction (U_o = 0.214 W/(m²·K)	4.4 kWh/m²	314
Moisture accumulation in the wall (maximum) after 10 years	26.5 kg/m²	50

TABLE 5 **Exercise 3: Material Properties**

w in kg/m³; u in %kg/kg; ϕ in –

Material	Property	Value Function					Units
lime silicate brick	density	1800					kg/m³
	specific heat capacity	850					J/(kg·K)
	thermal conductivity	0.9+0.0045w					W/(m·K)
	short-wave absorptivity	0.6					–
	sorption isotherm	ϕ					
		0	0				kg/m³
		0.5	16				
		0.8	27				
		0.9	43				
		0.93	57				
		0.96	139				
		0.99	232				
		0.999	245				
		0.9999	264				
		1	275				
	capillary moisture content	275					kg/m³
	saturation	350					kg/m³
	vapour permeability	$6.6\ 10^{-12}$					s
	water diffusivity	w	absorption		redistrib.		
		<20	0		0		
		20	1.5	10^{-10}	1.5	10^{-10}	
		82	1.3	10^{-9}	1.3	10^{-9}	
		179	–		2.0	10^{-9}	
		193	6.4	10^{-9}	–		
		275	2.0	10^{-7}	5.0	10^{-8}	
mineral fibre	density	60					kg/m³
	specific heat capacity	700					J/(kg·K)
	thermal conductivity	$0.04 + 0.0006w^5$					W/(m·K)
	vapor permeability	$1.2\ 10^{-10}$					s

peak concentration near and in the exterior wood fiberboard. The reasons for the large discrepancies in moisture accumulation may be whether or not latent heat transfer is considered and the way in which airflow is modeled.

Exercise 3: Cavity Wall

Data Common exercise 3, proposed by Germany, was composed of an intermodel comparison and an empirical verification (Künzel 1992, 1993). The objective of the exercise was to initiate two-dimensional modeling and to quantify the thermal and hygric impact of driving rain for cavity walls. The first part of the exercise therefore concerned a two-dimensional case: capillary water uptake and drying of a lime-silicate specimen measuring 49 cm (19.3 in.) high, 11 cm (4.3 in.) wide, and 7 cm (2.75 in.) deep, and sealed at the front, back, and one of the two sides. The cavity wall of the second part consisted of a 17.5 cm (6.9 in.) thick lime-silicate inner leaf; a cavity of 6 cm (2.4 in.), filled with mineral fiber; and a 11.5 cm (4.5 in.) thick lime-silicate outer leaf (Figure 1c). Material properties are given in Table 5. A weather data file for Holzkirchen was used. The indoor temperature was 20°C and the indoor relative humidity was 50%. Two cases were considered: wall airtight, wetted by precipitation; and wall airtight, no precipitation.

Expected Response For the lime-silicate specimen subjected to capillary rise and drying, fast wetting followed by slower drying was measured. In the cavity wall, hygric response should be dominated by rain absorption, as proven in practice.

Qualitative Verification of Simulation Results Eight reports with solutions were received. Glaser could only be used for the cavity wall. Application in accordance with British Standard BS 5250, German Standard DIN 4108, and the Belgian code of practice all classified the wall as of good design.

Solutions for the two-dimensional case with near-full models depict the response of the specimen during suction and drying as expected (see Figure 4). All gave faster wetting than drying. The same agreement between expected behavior and prediction is seen for the cavity wall. Driving rain builds up high moisture contents in the outer leaf. Drying in winter brings hardly any relief, whereas in summertime, the moisture content jumps between high after precipitation and low in between.

Numerical Verification of Simulation Results Table 6 compares the results for maximum water uptake in the specimen, maximum moisture content in the outer leaf in winter, and increase in U-factor of the cavity wall by rain. Figure 4 shows the calculated and measured wetting and drying curves for the specimen. Maximum water uptake for the specimen scatters substantially between the different simulations. The measured data also suggest an important secondary suction, caused by solution of entrapped air, which is missing in the calculations. Drying is simulated well in all reports.

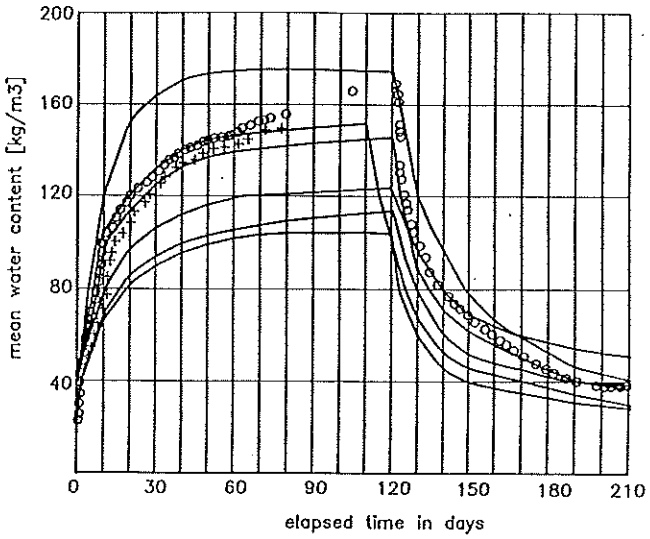

Figure 4 Exercise 3, comparison between the measured and calculated suction-drying curves for the 50 cm high lime-silicate specimen. The crosses and white dots are the measured data for two specimens. Each line represents a different simulation result.

TABLE 6 **Common Exercise 3: Maximal Mean Moisture Content in the Two-Dimensional Specimen, Maximal Mean Moisture Content in the Outer Leaf of the Cavity Wall, Increase in Heat Loss by Absorption of Driving Rain (Holzkirchen Climate, Germany)**

	Average (7 Reports)	Standard Deviation %
Maximal mean moisture content in the specimen (measured: 177 kg/m^3)	141 kg/m^3	20
Maximal mean moisture content in the outer leaf	222 kg/m^3	24
Increase in heat loss after 10 years	8.8%	31

The outer leaf of the cavity wall also is subjected to important discrepancies in predicted maximum moisture content. Even the peaks do not coincide. One of the reasons may be the different functional forms used to simulate the hygroscopic curve of the silicate-lime brick. Increase in U-factor, on the other hand, is predicted within narrow margins, with driving rain resulting in some 10% of extra losses, half latent heat, half conduction.

Exercise 4: Metallic Roof

Data Common exercise 4, proposed by the U.K., was an intermodel comparison (Nicholson and Johnson 1993a, 1993b), although a qualitative comparison with measured results was also included. The objective of the exercise was to evaluate the effects of air leakage through

TABLE 7 Exercise 4: Material Properties

Material	Property	Value Function	Units
		w in kg/m^3; u in kg/kg; ϕ in -	
steel profiled cladding	density	7850	kg/m^3
	thickness	1	mm
	thermal conductivity	68	W/(m·K)
mineral fibre	density	9.5	kg/m^3
	thermal conductivity	0.039 + 0.0084u	W/(m·K)
	sorption isotherm	$u_h(1 - \ln\phi/A)^{-1/n}$ adsorption: u_h = 0.0545 1/n = 0.211 A = 0.000548 desorption: u_h = 0.14 1/n = 0.318 A = 0.0005011	kg/kg
	vapour permeability	1.4 10^{-10}	s
steel liner tray	density	7850	kg/m^3
	thickness	0.5	mm
	thermal conductivity	68	W/(m·K)

the liner, outside air ventilation in the cavity, and clear sky undercooling on the hygrothermal response of a noncapillary, lightweight cold-deck structure. The metallic roof proposed consisted of an interior steel liner tray, an 80 mm (3.1 in.) thick fiberglass quilt, and a steel-profiled cladding, with the separation between tray and cladding being maintained with Z-spacers (Figure 1d). Material properties are given in Table 7. The first case considered was a hot-box experiment on a roof measuring 1.5 m wide and 2 m long, with a slope from ridge to eave of 6 degrees, and all openings at both ridge and eaves filled with foam inserts. Conditions were: inside 15°C, 65% RH; outside, successively, 15°C/65%, 10°C/75%, and 5°C/90%. In the second case, the roof covered a small building measuring 5 m wide and 10 m long. The slope was 6 degrees. A weather data file for Manchester was used. The indoor temperature was 15°C, and the indoor relative humidity was 65%.

Expected Response Metallic roofs are sensitive to undercooling by longwave clear-sky losses. This should change the external air in the cavity into a moisture source rather than a drying flow. Exfiltration, in turn, may aggravate cavity condensation. The overall result: a larger sensitivity to interstitial condensation and a faster reaction to climatic changes than simple engineering tools predict.

Qualitative Verification of Simulation Results Nine reports with solutions were received. A Glaser prediction gave no accumulation of condensate on a yearly basis. The winter maximum, however, was too high, which degraded the structure to that of "unacceptable moisture design."

Solutions with simplified or near-full models taught that even a metallic roof with mineral fiber insulation has some thermal and hygric inertia. Exfiltration, however, reduces the time lag to a fraction of the value without exfiltration. For the small building, air leaks more than double condensation in the roof compared to an airtight construction. Although summer drying still prohibits accumulation, reversed condensation on the metallic tray becomes a point of concern.

TABLE 8 Common Exercise 4: Total Yearly Condensation at the Underside of the Cladding (Manchester Climate, U.K.)

	Average (6 Reports)	Standard Deviation %
Total yearly condensation when diffusion is the only vehicle for vapour ingress	0.23 kg/m^2	45
Total yearly condensation with air leaks in the liner	0.54 kg/m^2	90

Numerical Verification of Simulation Results Measured vapor pressure curves in the air space between the tray and mineral wool were not self-explaining enough to be used as a reference. Verification therefore was restricted to an intercomparison. Table 8 gives the results for maximum condensation in winter with and without air leaks. The high standard deviation for the leaky case shows that calculation of air leak surfaces from monitored flows introduces major uncertainties. One, in fact, has to translate fluxes into a balanced set of air permeabilities of tray, cavity ends, and cladding.

Exercise 5: Timber Flat Roof

Data Common exercise 5, proposed by Denmark, was a mixed-type intermodel comparison and empirical verification (Rode 1993, 1994). The objective of the exercise was to reproduce the experimental results gained on four timber test roofs. These consisted of (from inside to outside): 25 mm (1 in.) of wood-wool cement board, either a 0.15-mm (0.06-in.) polyethylene foil (called PE) or a water-permeable vapor retarder, 10 cm (3.9 in.) of mineral fiber insulation, an air space with a height of 95 mm (3.7 in.), a 12.5 mm (0.49 in.) thick plywood deck, and an SBS-modified membrane (Figure 1e). Material properties were measured by the participants. For that purpose, samples were distributed together with a weather file containing the measured indoor and outdoor climates. Four cases were considered: PE-vapor retarder, no initial moisture; PE-vapor retarder, initial moisture; water-permeable vapor retarder, no initial moisture; and water-permeable vapor retarder, initial moisture. Initial moisture consisted of a few layers of cellulose cardboard sprayed with 3 kg/m^2 of moisture and added on top of the thermal insulation. At the start, all other layers were in equilibrium with 60% RH.

Expected Response The vapor retarders used have quite different properties: PE is vapor tight, while the water-permeable retarder combines a medium vapor resistance with a wicking action each time summer con-

densation forms on its surface. One could therefore expect that initial moisture should dry faster in the roof with the water-permeable vapor retarder than in the roof with the PE-vapor retarder. On the other hand, in winter, more interstitial condensation should be expected with the water-permeable retarder. Experimental results, however, did not confirm that pattern: drying of initial moisture went on much slower than expected with the water-permeable vapor retarder and condensation was as pronounced with the PE-vapor retarder as with the water-permeable type.

Qualitative Verification of Simulation Results Nine reports with solutions were received. Application of the Glaser method showed that, with the environmental conditions imposed, neither the roof with a PE-vapor retarder nor the roof with a water-permeable vapor retarder demonstrated unacceptable interstitial condensation. Both were of "good moisture design."

Solutions with simplified or near-full models, on the other hand, all confirmed the expected pattern: faster drying of built-in moisture with the water-permeable vapor retarder, and less interstitial condensation in the roofs with the PE-foil. None of the simulations produced the measured results, except if a low vapor resistivity for both vapor retarders was used, or if indoor air leakage into the cassettes was accepted. Even a two-dimensional analysis failed in explaining the measurements. The probable conclusion therefore is, opposite to what the researchers took for granted at the start of their experiments, the roof cassettes suffer from indoor air leakage.

Numerical Verification of Simulation Results Figure 5 compares seven solutions for the "water-permeable vapor retarder, initial moisture" case. Differences between total moisture contents are important. One solution even gives a completely different picture, with a much larger increase between summer and winter and lower values in summer. This seemed to be caused by differences in the functional relationships used for the material properties. On the other hand, heat fluxes coincided well (Table 9).

TABLE 9 **Common Exercise 5: Average Heat Flux Through the Four Flat Timber Roofs (Copenhagen Climate, Denmark)**

	Average (7 Reports)	Standard Deviation %
Average heat flux, PE-foil, dry	2.7 W/m^2	36
Average heat flux, PE-foil, initial moisture	2.9 W/m^2	18
Average heat flux, water permeable vapour retarder, dry	2.8 W/m^2	33
Average heat flux, water permeable vapour retarder, initial moisture	2.8 W/m^2	23

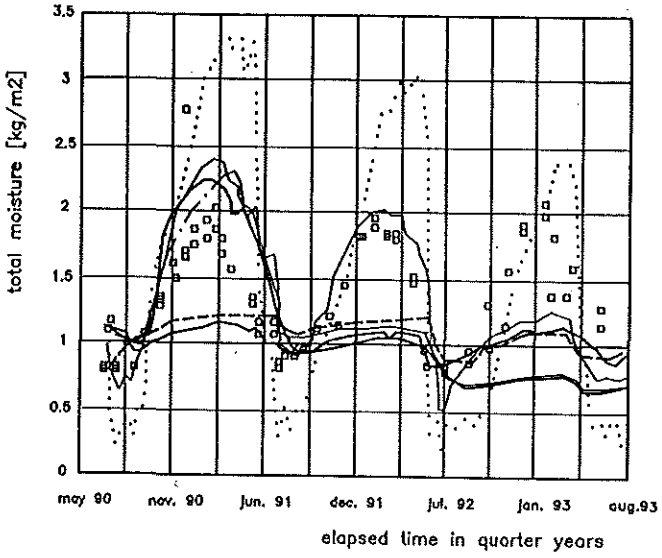

Figure 5 Exercise 4, comparison between the calculated and measured moisture content in the timber roof cassettes with water-permeable vapor retarder and initial moisture. The white squares are the measured data. Each line represents a different simulation result. The dotted line with largest amplitude is calculated with a low vapor resistance of the retarder.

Exercise 5 also deals with material properties. Three laboratories measured the vapor diffusion resistances of the PE-foil, the water-permeable vapor retarder, plywood, and wood-wool cement. For PE, the water-permeable vapor retarder, and plywood, results were close. For wood-wool cement, one laboratory ended with a high vapor permeability, while the other two found a much lower value (see Figure 6).

Exercise 6: Crawl Space

Data Common exercise 6, proposed by Sweden, was an intermodel comparison (Hagentoft 1994). The objective of the exercise was to judge, on efficiency, two means for lowering the relative humidity in a crawl space: a ground cover and ground insulation. The two vented crawl spaces had a surface of 10.9 by 12.2 m for a height of 1.5 m (0.9 m below grade and 0.6 m above grade). All perimeter walls are 30 cm thick. The water table is 1 m below grade. The type of soil is moraine, with λ = 2.3 W/(m·K) and ρc = 2.0 10^6 J/(m^3·K). The floor construction consists of (from crawl space to inside): 6 mm (0.24 in.) of hardboard, 22 cm (8.7 in.) of mineral fiber, and 22 mm (0.9 in.) of timber flooring (Figure 1f). In one of the crawl spaces, the bottom is covered with a 0.15-mm-thick PE film. In the other, the ground is protected by a 30 cm (11.8 in.) thick lightweight aggregate loose fill, λ = 0.13 W/(m·K), δ_v = 7.10^{-6} m^2/s. A

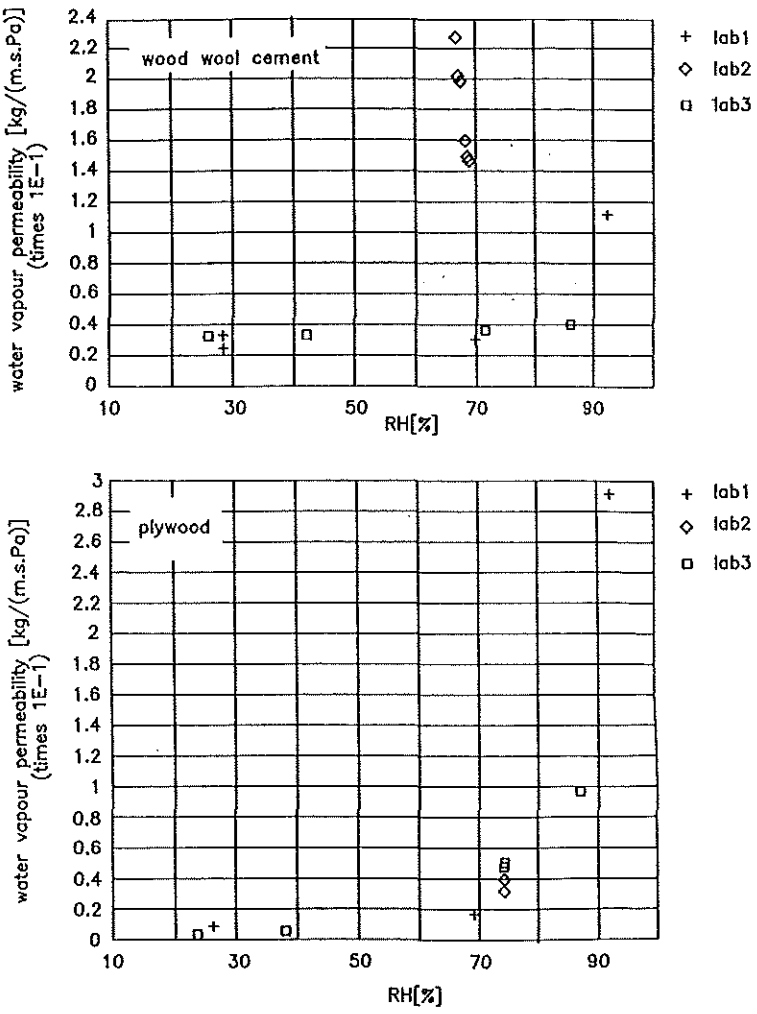

Figure 6 Exercise 5, measured vapor permeabilities of plywood and wood wool cement board, data of three laboratories (crosses, white squares, rhombs).

weather file containing the measured indoor and outdoor climatic data was used. Four cases were considered: a crawl space with PE-ground cover, measured climatic data; a crawl space with PE-ground cover, monthly average climatic data and an indoor temperature of 20°C; a crawl space with loose-fill ground cover, measured climatic data; and a crawl space with loose-fill ground cover, monthly average climatic data, and an indoor temperature of 20°C.

Expected Response The vapor-permeable, loose-fill ground cover of 30-cm expanded clay aggregate is expected to result in higher air temperatures and higher relative humidities than the PE ground cover.

Qualitative Verification of Simulation Results Six reports with solutions were received. Solutions with simplified models, as well as with near-full models, showed a large scatter. Some confirmed the expectations, others predicted small differences between both cases, and some ended with a warmer and drier crawl space with loose fill on the bottom. The reasons for these opposite answers are manifold: differences in ventilation rate in the crawl space, differences in location of the ground-isotherm below grade (1 m, 3 m, 10 m), underestimation of the vapor leakage at the perimeter of the PE foil, etc.

Numerical Verification of Simulation Results Qualitative differences between solutions are too large to allow any numerical verification. However, a comparison with the measured response showed that even a one-dimensional periodic solution with yearly average and yearly amplitude could perform in a satisfactory way if a correct ventilation rate was introduced, if the ground-isotherm was located correctly, and if vapor leakage at the perimeter was taken into account. In the absence of these, even three-dimensional models deviate substantially from the measured response.

CONCLUSIONS

The following conclusions emerged from the Annex 24 verification work on heat, air, and moisture transfer models, using the six common exercises as vehicles.

1. Simple steady-state engineering tools have a restricted capability as design instruments. In many cases, they do not even succeed in giving a correct answer to the question: Is the design acceptable or not? This is demonstrated in exercises 1, 2, 3, and 5: the Glaser rationale, as implemented in standards and codes of practice, declares the construction as being of "good moisture design," where in reality initial moisture, precipitation, and air exfiltration cause many problems.
2. The exercises confirm the following order of importance for the hygrothermal behavior of envelope parts: (1) air exfiltration, (2) initial moisture, (3) latent heat, and (4) precipitation. Air exfiltration impairs the hygrothermal response completely. If present, all rules on correct vapor resistance division between interior lining and exterior cladding become obsolete, as proven by exercise 2. Hot-box and field measurements show one should also add air rotation to the list. Modeling this phenomenon, however, demands two- and three-dimensional approaches (Janssens et al. 1992; Ojanen et al. 1994).
3. In most cases, simplified to near-full models produce a correct hygrothermal response, at least from a qualitative point of view. This, of course, only is true if all mass transport modes, thermal and hygric inertia, conduction, enthalpy flow, latent heat, and correct starting and boundary conditions are considered. If not, these models fail for cases where the neglected phenomenon dominates hygrothermal behavior.
4. Large differences remain between the numerical results. Major reasons include simplification of material properties, different interpretations of boundary conditions, and differences in geometry. Examples of the

first reason are found in sorption isotherms and diffusivity. The choice of a specific functional form for the sorption isotherm may lead to important differences in moisture content between 90% and 100% relative humidity, the interval where suction-driven water flow becomes active. Diffusivity vs. moisture content, in turn, defines the moisture profile in this relative humidity interval in all capillary-porous layers. Hence, for many materials, the correct diffusivity vs. moisture relation is not known. This forces one to simplify. An example of the second reason is given by the crawl space exercise, where the ventilation rate had to be guessed by the participants. Its influence on temperature and relative humidity in the crawl space, however, is preponderant. An example of the third reason again is found in the crawl space exercise. The PE foil is applied between the foundation walls. This results in important perimeter leaks. If these are not taken into account, relative humidity is calculated for a situation that is too positive.

5. Verification was restricted to temperatures, fluxes, total energy flows, and time-integrated quantities such as moisture content and condensate. As soon as moisture profiles, for example, are compared, numerical differences become even more pronounced.

To summarize, the actual level of modeling is such that, in many cases, a good qualitative picture of reality is produced. In airtight envelope elements, prediction of the variation of the moisture content in the different layers may even be a success numerically. This, however, does not exclude that more partial verification and, if possible, real validation of heat, air, and moisture models is needed. The focus in the annex, for example, was restricted to one-dimensional problems. Reality, however, is three-dimensional. A restricted set of materials was used, i.e., only mineral fiber as insulation material. Anisotropy was not introduced. Hence, the collection of building, insulating, and finishing materials is large, and purely isotropic materials are an exception. Air movement is fitted into simple one- or two-dimensional networks: exfiltration, infiltration, and/or ventilation. Real air movement networks, on the contrary, are in most cases three-dimensional. As a start, a compilation of analytical solutions for single systems, multilayered systems, and simple two-dimensional problems could be produced as a tool to verify algorithms. Then well-documented, measured benchmark examples should be distributed on disk. Finally, further intermodel comparisons are needed, for example, as round-robin activity in the frame of CIB-W40, ASHRAE, and other international organizations.

ACKNOWLEDGMENTS

The paper is the result of a joint research effort within the frame of Annex 24. We thank all participants in the annex for their enthusiastic cooperation. We also thank the Flemish government for the financial support in accomplishing the task of being the operating agent of Annex 24.

NOMENCLATURE

g = acceleration by gravity (m/s^2)
h = specific enthalpy (J/kg)
k_w = water flux (vector, kg/[m^2·s])
k_a = air permeability (s)
l_b = latent heat for evaporation (J/kg)
m_v =water vapor flux (vector, kg/[m^2·s])
m_v = water flux (vector, kg/[m^2·s])
m_a = air flux (vector, kg/[m^2·s])
p = vapor pressure (Pa)
p_a = total air pressure (Pa)
q = heat flux (vector, W/m^2)
s = suction (Pa) (for example, capillary suction)
u = moisture ratio (%kg/kg)
w = moisture content (kg/m^3)
A = water sorption coefficient (the slope of the water uptake per unit surface vs. square root of time straight line, as obtained from a suction test
S = rate of generation or absorption, $_Q$ for heat, $_M$ for moisture (quantity/[m^3·s])
T = temperature (K)
X = water vapor ratio (kg/kg)
δ = vapor permeability (s)
λ = thermal conductivity (W/[m·K])
ρ = density (kg/m^3)
ϕ = relative humidity
div $= \left(= \frac{\partial}{\partial x} + \frac{\partial}{\partial y} + \frac{\partial}{\partial z} \right)$ divergence operator for vectors
grad $= \left(= \frac{\partial}{\partial x} + \frac{\partial}{\partial y} + \frac{\partial}{\partial z} \right)$ gradient vector operator for scalars
bold = vectors

REFERENCES

Anon. 1991. *Official text for the annex on heat, air and moisture transfer in highly insulated, new and retrofitted envelope parts.*

Galbraith, G.H., R.C. McLean, and Z. Tao. 1991. BCR programme, intercomparison on measurements of water vapour permeability. Final Report Project 3366/1/0/151/90/1-BCR-UK(30), edited by the University of Strathclyde.

Glaser, H. 1958. Vereinfachte Berechnung der dampfdiffusion durch geschichtete Wände bei Ausscheiden von Wasser und Eis. *Kältetechnik*, 11: 358-364, 12: 345-349.

Hagentoft, C.E. 1994. Common exercise 6, crawl-space with and without ground insulation. Exercise text, Internal Report T1-S-94/02, Annex 24.

Hens, H. 1991. First common exercise: Heavy flat roof with mineral wool insulation. Internal Report T1-B-91/05, Annex 24.

Hens, H. 1992. First common exercise: Concrete flat roof with mineral wool insulation. Summary Report, Internal Report T1-B-92/02, Annex 24.

Janssens, A., H. Hens, A. Silberstein, and J. Boulant. 1992. The influence of underroof systems on the hygrothermal

behaviour of sloped insulated roofs. *Proceedings of the Thermal Performance of the Exterior Envelopes of Buildings V Conference*, Clearwater Beach, Fla., December 7-10, pp. 368-378.

Kumaran, M.K. 1992a. Report on measurements to determine moisture diffusivity of eastern white pine. Internal Report T3-CA-92/03, Annex 24.

Kumaran, M.K. 1992b. Report on analytical methods to derive moisture diffusivity from transient moisture distribution. Internal Report T3-CA-92/04, Annex 24.

Künzel, H. 1992. Third common exercise: Calculation of the 2-dimensional moisture transfer in a lime-sandstone specimen and of the 1-dimensional heat and moisture transfer in a cavity wall. Internal Report T1-D-92/07, Annex 24.

Künzel, H. 1993. Results of the third common exercise. Internal Report T1-D-93/02, Annex 24.

Lomas, K.J. 1994. Thermal programme validation. *Proceedings of the BEP 94 Conference*, pp. 73-82.

Nicholson, P.J., and K.A. Johnson. 1993a. Fourth common exercise. Internal Report T1-UK-93/01, Annex 24.

Nicholson, P.J., and K.A. Johnson. 1993b. Fourth common exercise–External roof results: Heat, air and moisture transfer in industrial roofs. Internal Report T1-UK-93/03, Annex 24.

Ojanen, T., and M. Salonvaara. 1992a. Second common exercise: 1-dimensional air flow through a wall structure. Internal Report T1-SF-92/02, Annex 24.

Ojanen, T., and M. Salonvaara. 1992b. Summary report, second common exercise: 1-dimensional air flow through a wall structure. Internal Report T1-SF-92/03, Annex 24.

Ojanen, T., R. Kohonen, and K. Kumaran. 1994. Modelling heat, air and moisture transport through building materials and components. *Moisture Control in Buildings*, pp. 18-34. Philadelphia, Pa.: American Society for Testing and Materials.

Rode, C. 1993. Fifth common exercise: Moisture conditions of non-ventilated, wood-based membrane roof components. Internal Report T1-Dk-93/02, Annex 24.

Rode, C. 1994. Fifth common exercise: Solutions. Internal Report T1-Dk-94/01, Annex 24.